Magnetic field induced effects in the quasikagome Kondo lattice system CePtPb

A. C. Y. Fang,[1] S. R. Dunsiger,[1] A. Pal,[1] K. Akintola,[1] J. E. Sonier,[1,2] and E. Mun[1]
[1]*Department of Physics, Simon Fraser University, Burnaby, British Columbia, Canada V5A 1S6*
[2]*Canadian Institute for Advanced Research, Toronto, Ontario, Canada M5G 1Z8*

(Received 23 March 2019; published 2 July 2019)

The Kondo lattice compound CePtPb crystallizes in the ZrNiAl-type structure with the space group $P\bar{6}2m$, where the Ce^{3+} ions form a quasikagome lattice in the *ab* plane. We have constructed a temperature versus magnetic field (T-H) phase diagram for single-crystal CePtPb from electrical resistivity and specific heat measurements. Our results indicate the occurrence of long-range antiferromagnetic order below $T_N = 0.95$ K and multiple magnetically ordered phases as T_N is suppressed by applied magnetic field. Although T_N can be continuously suppressed to zero by the field, the resistivity and specific heat close to the critical field $H_c \approx 6$ kOe do not follow simple models of quantum criticality. Above H_c, the electrical resistivity shows an unconventional T^n dependence with $n > 2$. We also present muon spin relaxation measurements, which reveal residual spin dynamics below T_N that are consistent with only two thirds of the Ce-4f spins participating in the antiferromagnetic order.

DOI: 10.1103/PhysRevB.100.024404

I. INTRODUCTION

Heavy fermion (HF) metals have became prototypical systems to study quantum criticality, because these systems host various ordered phases and are easily tunable [1,2]. The ground state of HF compounds is governed by the competition between the Kondo coupling and Ruderman-Kittel-Kasuya-Yoshida (RKKY) exchange interactions between the localized 4f moments, leading to paramagnetic, heavy Fermi liquid and ordered magnetic states [3]. The balance between these interactions can be tuned by chemical substitution, external pressure or applied magnetic field to drive the ground state from a long-range magnetically ordered phase to a paramagnetic state through a quantum critical point (QCP) [4,5]. It has been shown that non-Fermi liquid (NFL) behavior with a divergent effective quasiparticle mass occurs near the QCP [4–6]. In addition to the competition between the Kondo and RKKY interactions, it has been suggested that magnetic order may also be tuned by the introduction of magnetic frustration (quantum fluctuations) [7–13]. Thus unconventional quantum criticality can occur via the interplay between the Kondo and RKKY interactions and magnetic frustration.

The effect of geometrical frustration on a Kondo lattice system has been studied in hexagonal ZrNiAl-type structures, such as YbAgGe [14–18], CePdAl [19–24], and CeRhSn [25–27], where the trivalent rare-earth ions form a frustrated quasikagome lattice in the *ab* plane. In YbAgGe, successive magnetic transitions are observed as the Néel temperature T_N is suppressed by applied magnetic field, eventually to zero at a QCP [15–17]. A wide range of NFL behavior and quantum bicritical scaling has been related to geometric frustration [18]. In CePdAl, neutron scattering and nuclear magnetic resonance (NMR) experiments indicate that only two thirds of the Ce-4f moments order antiferromagnetically below 2.7 K, while due to geometrical frustration, the other third remain paramagnetic down to 50 mK [20,21]. Although there is a rich field-induced progression of some of the physically observable quantities for CePdAl at low temperature, standard signatures of NFL behavior are not observed near the putative QCP [22,23]. The partial magnetic order in CePdAl can be suppressed by substituting Pd with Ni, resulting in a logarithmic divergence of the ratio of the specific heat to temperature C_p/T at a critical Ni concentration—which is a signature of NFL behavior [24]. In the isostructural compound CeRhSn, the temperature dependence of the magnetic susceptibility and electrical resistivity exhibit NFL behavior [25], likely due to a zero-field QCP induced by geometrical frustration [27].

While the interaction of the conduction electrons with frustrated magnetism in a HF system provides an intriguing possibility to observe unusual states of matters, there are not many candidate systems to study. Hence, it is desirable to study new HF compounds with optimal conditions for magnetic frustration. CePtPb is another isostructural Kondo lattice system that crystallizes in the hexagonal ZrNiAl-type structure [28]. In an earlier report [28], magnetization, zero-field electrical resistivity, and zero-field specific heat measurements on CePtPb revealed the onset of antiferromagnetic order below $T_N = 0.9$ K, a Sommerfeld coefficient $\gamma = 300\,\mathrm{mJ\,mol^{-1}\,K^{-2}}$, and a large frustration ratio $f = \theta_p/T_N \approx 44$, where θ_p is the Curie-Weiss temperature. Motivated by previous studies of ZrNiAl-type compounds, we have grown and characterized single crystals of CePtPb by magnetization, electrical resistivity, specific heat, and muon-spin relaxation (μSR) measurements in a wide range of temperature and magnetic field. The T-H phase diagram is constructed from resistivity and specific heat measurements down to 0.4 K and up to 90 kOe. A systematic analysis of the power-law behavior of the resistivity indicates that the antiferromagnetic order does not vanish at a conventional QCP. Our μSR measurements down to 20 mK reveal residual spin dynamics below T_N that are indicative of magnetic frustration. These findings provide additional information for understanding the

 ©2019 American Physical Society

influence of magnetic frustration on quantum criticality in HF systems.

II. EXPERIMENTAL

Single crystals of CePtPb and LaPtPb were grown in a Pb-rich ternary melt [28,29]. Powder x-ray diffraction measurements were performed in a Rigaku MiniFlex at room temperature. The peak positions in the powdered pattern can be indexed with a hexagonal ZrNiAl-type structure with lattice parameters $a = 7.730(4)$ Å and $c = 4.126(8)$ Å for CePtPb and $a = 7.774(4)$ Å and $c = 4.168(3)$ Å for LaPtPb. These lattice constant values are consistent with an earlier study [28]. The crystallographic directions were determined by Laue diffraction. The dc magnetization as a function of temperature and magnetic field was measured with a Quantum Design (QD) Magnetic Property Measurement System (MPMS) from 1.8 to 300 K and up to 70 kOe. The temperature and magnetic field dependence of the resistivity were measured in a QD Physical Property Measurement System (PPMS) by the ac ($f = 17$ Hz) method up to 90 kOe. The specific heat was measured from 0.4 K to 300 K by the relaxation method in a QD PPMS. μSR experiments performed at TRIUMF in an Oxford Instruments Model 400 dilution refrigerator. Zero-field (ZF) μSR measurements of CePtPb were performed between 25 mK and 3 K on a mosaic of c-axis aligned single crystals mounted on a silver (Ag) sample holder, with the initial muon-spin polarization $\mathbf{P}(t = 0)$ perpendicular to the c axis. In addition, longitudinal-field (LF) μSR measurements were carried out for magnetic fields up to 9 kOe applied perpendicular to the c axis.

III. RESULTS

A. Magnetization

Figure 1 shows the magnetic field dependence of the magnetization $M(H)$ for LaPtPb at $T = 2$ K for a field applied parallel to the c axis ($H \parallel c$). The gradual decrease in $M(H)$ with increased magnetic field is indicative of a weak diamagnetic response. The temperature dependence of the magnetic susceptibility $\chi(T) = M(T)/H$ for a field $H = 70$ kOe applied parallel to the c axis is shown in the inset of Fig. 1. Between 300 and 100 K, $\chi(T)$ linearly decreases with decreasing temperature. Below 100 K, $\chi(T)$ exhibits an upturn, most likely due to paramagnetic impurities.

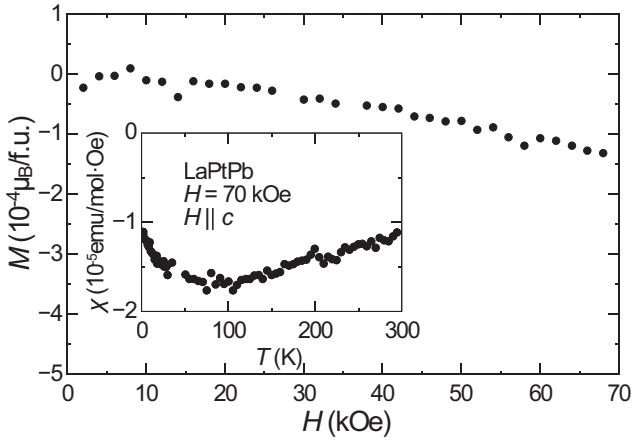

FIG. 1. Magnetic field dependence of the magnetization of LaPtPb at $T = 2$ K for $H \parallel c$. Inset shows the temperature dependence of the magnetic susceptibility at $H = 70$ kOe.

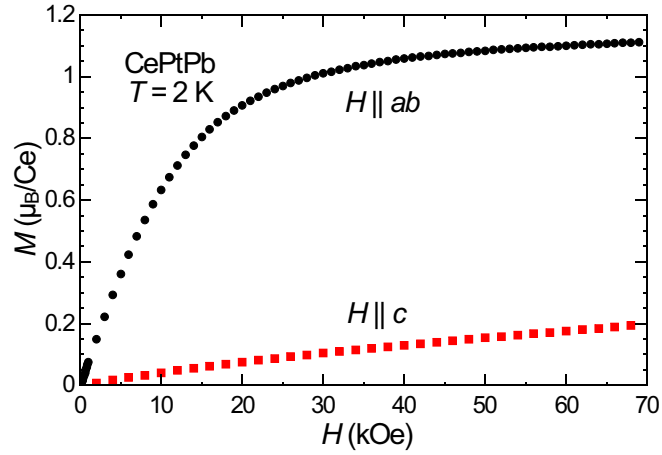

FIG. 2. Magnetic field dependence of the magnetization of CePtPb at $T = 2$ K for both $H \parallel ab$ and $H \parallel c$.

Figure 2 shows $M(H)$ data for CePtPb at $T = 2$ K. The ab-plane magnetization $M_{ab}(H)$ shows a tendency towards saturation as the magnetic field increases from 30 to 70 kOe, whereas the c-axis magnetization $M_c(H)$ continues to increase quasilinearly with magnetic field up to 70 kOe. At $T = 2$ K and $H = 70$ kOe, $M_{ab}(H)$ and $M_c(H)$ reach values of $\approx 1.1\,\mu_B$/Ce and $\approx 0.2\,\mu_B$/Ce, respectively, which are smaller than the saturation value ($gJ = 2.14\,\mu_B$) for a free Ce^{3+} ion. The large anisotropy between $M_{ab}(H)$ and $M_c(H)$ and the reduction in magnetization are due to the effect of the crystalline electric field (CEF) and Kondo screening.

The temperature dependence of the inverse magnetic susceptibility $1/\chi(T)$ for CePtPb is shown in Fig. 3. Our

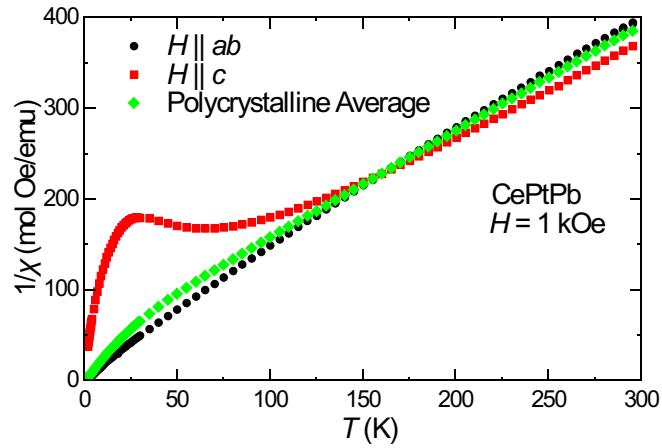

FIG. 3. Temperature dependence of the inverse magnetic susceptibility of CePtPb at $T = 2$ K for a field $H = 1$ kOe applied parallel to the ab plane and to the c axis. The green diamond symbols represent the calculated polycrystalline average.

data for $1/\chi(T)$ and $M(H)$ are consistent with an earlier study of CePtPb [28]. The polycrystalline average, defined as $\chi_{\rm avg}(T) = 2/3\chi_{ab} + 1/3\chi_c$ (where χ_{ab} and χ_c are the magnetic susceptibilties for fields applied parallel to the ab plane and the c axis, respectively) is displayed in Fig. 3. Above 150 K, the magnetic susceptibility follows the Curie-Weiss behavior $\chi(T) = C/(T-\theta_p)+\chi_0$, where C is the Curie constant, θ_p is the Curie-Weiss temperature, and χ_0 is a background contribution. The effective moment obtained from the fitted value of C for all three data sets in Fig. 3 is close to the Ce free ion value of $2.54\,\mu_{\rm B}$, suggesting the ground state of the Ce ions in CePtPb is $J = 5/2$. The fitted values of χ_0 are on the order of 10^{-5} emu/mol, in agreement with the magnetic susceptibility of isostructural LaPtPb. The fitted values of θ_p for $H \parallel ab$, $H \parallel c$, and the polycrystalline average are -33, -51, and -38 K, respectively. The negative sign suggests an antiferromagnetic (AFM) ground state, and the values of θ_p are in good agreement with the earlier study [28]. The large absolute value of the frustration ratio $|f| \approx 40$ inferred from the polycrystalline average value $\theta_p \approx -38$ K and $T_{\rm N} = 0.95$ K (see below) suggests that magnetic interactions in CePtPb are geometrically frustrated. However, this ratio can be easily influenced by the Kondo and CEF effects. Below 150 K, a strong anisotropy develops between $\chi_{ab}(T)$ and $\chi_c(T)$. The ratio χ_{ab}/χ_c increases continuously as the temperature decreases to a value near 17 at $T = 2$ K .

B. Electrical resistivity

The temperature dependence of the electrical resistivity $\rho(T)$ for CePtPb is displayed in Fig. 4(a). As the temperature is lowered from 300 K, $\rho(T)$ decreases with decreasing temperature, indicating metallic-like behavior. At low temperatures, $\rho(T)$ shows a broad hump [Fig. 4(b)], which is typically observed in a Kondo-lattice system. A kink in $\rho(T)$ is observed near 0.95 K [Fig. 4(c)], which coincides with the AFM transition. We note that an upward kink in $\rho(T)$ was previously observed near $T_{\rm N}$ [28]. Below $T_{\rm N}$, the resistivity exhibits a cubic dependence on temperature: $\rho(T) = \rho_0 + AT^n$ with $\rho_0 = 5.56\,\mu\Omega\,$cm, $A = 0.28\,\mu\Omega/{\rm K}^3$ and $n = 3$ [Fig. 4(d)]. The fitted value of ρ_0 is over four times smaller than that determined in Ref. [28]. Furthermore, the residual resistivity ratio RRR $= \rho(300\,{\rm K})/\rho(0.4\,{\rm K})$ is approximately 6.2, compared to nearly 2.5 in the earlier study. Hence the CePtPb single crystals investigated in the current study are apparently of higher quality. The fitted value $n \approx 3$ is also different from the earlier reported value $n = 2$ [28].

Figure 4(e) shows $\rho(T)$ for various magnetic fields applied in the ab plane. The AFM order determined by the slope change in $\rho(T)$ is continuously suppressed to lower temperature as the magnetic field is increased. For $H = 3.25$ and 3.5 kOe, two slope changes and thermal hysteresis are observed, which are indicative of phase transitions. As the magnetic field is increased from 10 to 90 kOe, the resistivity approaches saturation at low temperatures [Fig. 4(f)], indicating an anomalous power-law dependence on temperature.

Figures 5(a) and 5(b) show the magnetic field dependence of the electrical resistivity $\rho(H)$ for $H \parallel ab$. Above $T_{\rm N}$, the resistivity gradually decreases as the magnetic field is increased, whereas below $T_{\rm N}$, $\rho(H)$ exhibits multiple anomalies

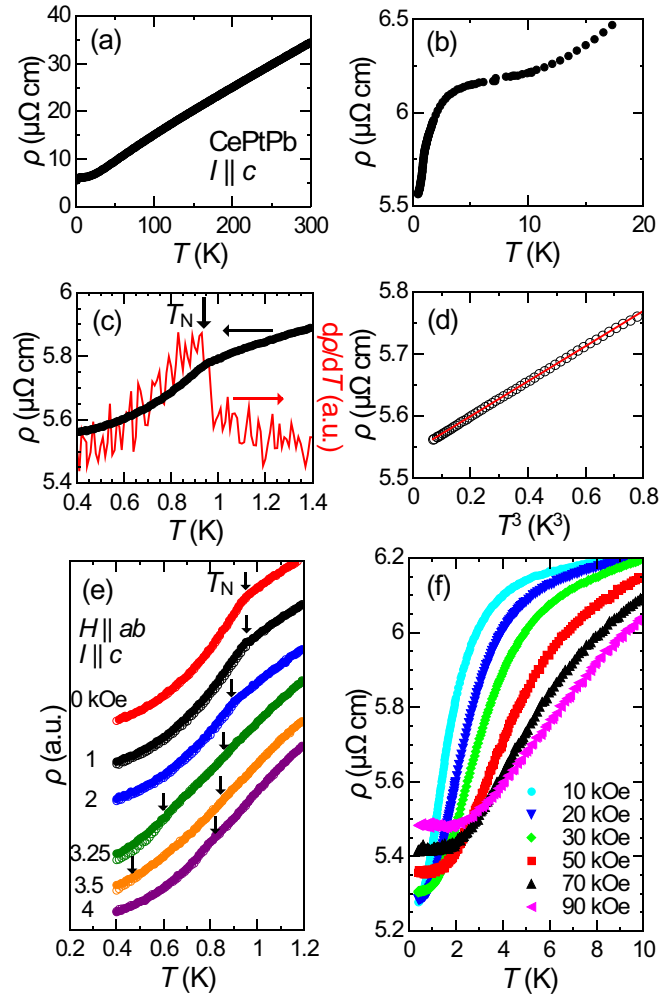

FIG. 4. (a) The temperature dependence of the electrical resistivity $\rho(T)$ for CePtPb in zero field. (b) $\rho(T)$ below 20 K. (c) $\rho(T)$ (left axis) and $d\rho(T)/dT$ (right axis) below 1.4 K. The vertical arrow indicates $T_{\rm N} = 0.95$ K. (d) $\rho(T)$ below $T_{\rm N}$ plotted as a function of T^3. The solid red line is a linear fit to the data. (e) $\rho(T)$ for $H \parallel ab$ measured as a function of increasing (open circles) and decreasing (solid circles) temperature. The vertical arrows indicate the magnetic ordering temperature. The individual data sets are offset for clarity. (f) $\rho(T)$ between 10 and 90 kOe for $H \parallel ab$.

with hysteresis. At $T = 0.4$ K, $\rho(H)$ changes little between 0 and 2 kOe with a slight increase above $H \approx 0.8$ kOe. As the magnetic field is further increased, $\rho(H)$ exhibits a rapid decrease above $H \approx 2$ kOe and a broad hump around 3.6 kOe. In addition, hysteresis is observed between 0.8 and 3.6 kOe and a slope change in $\rho(H)$ is observed near 6 kOe. As the temperature is increased, the slight increase near 0.8 kOe persists and the broad hump around 3.6 kOe and the slope change near 6 kOe gradually shift to lower magnetic field. Figure 5(b) shows $\rho(H)$ up to 90 kOe at selected temperatures. At $T = 5$ K a negative magnetoresistance is observed up to 90 kOe, whereas below 2 K the magnetoresistance changes sign from negative to positive in the high-field regime. At $T = 0.4$ K, $\rho(H)$ exhibits a linear dependence on magnetic field for $H > 20$ kOe.

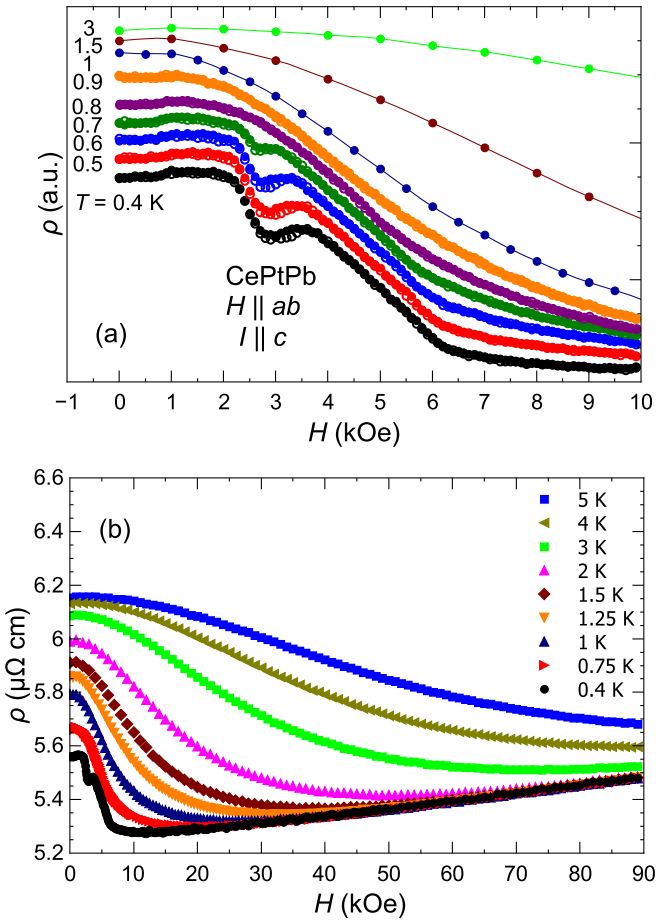

FIG. 5. Magnetic field dependence of the electrical resistivity $\rho(H)$ for CePtPb (a) up to 10 kOe measured as a function of increasing (open circles) and decreasing (closed circles) magnetic field, and (b) up to 90 kOe at selected temperatures.

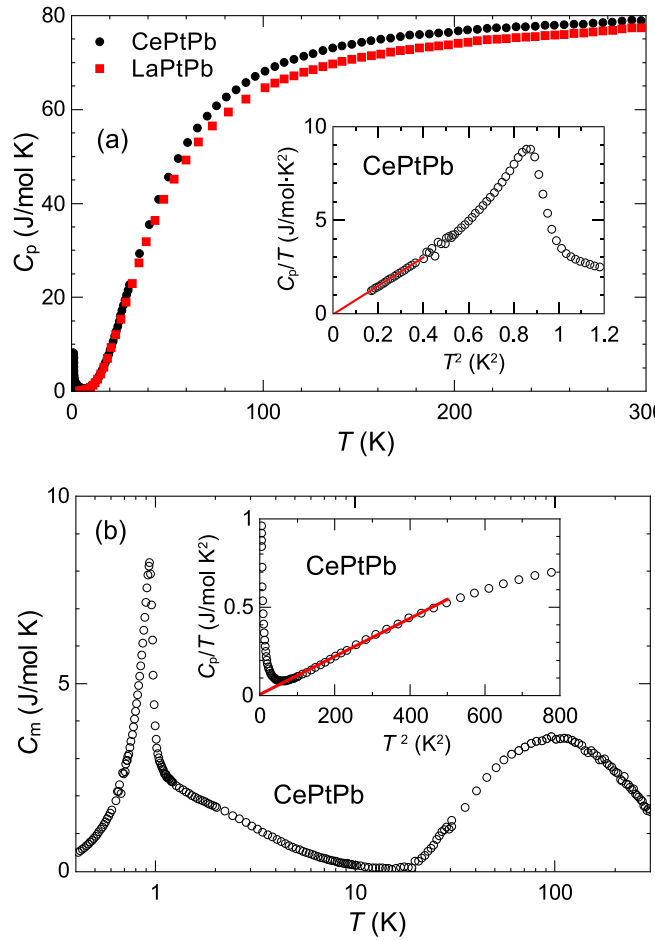

FIG. 6. (a) Temperature dependence of the specific heat $C_p(T)$ for CePtPb and LaPtPb at $H = 0$ kOe. The inset shows a plot of C_p/T vs T^2. The solid red line is a linear fit between 0.16 K^2 and 0.4 K^2. (b) Magnetic contribution C_m to the specific heat of CePtPb. The inset shows a plot of C_p/T vs T^2. The solid red line is a linear fit between 65 and 500 K^2.

C. Specific heat

The temperature dependence of the specific heat $C_p(T)$ for CePtPb and LaPtPb are shown in Fig. 6(a). The overall temperature dependence of the specific heat for LaPtPb is similar to that of ordinary metals. At low temperatures, $C_p(T)$ of LaPtPb is well described by $C_p(T) = \gamma T + \beta T^3$, which yields a Sommerfeld coefficient $\gamma = 3.9$ mJ mol^{-1} K^{-2} and Debye temperature $\Theta_D \approx 180$ K. The specific heat for CePtPb shows a sharp pronounced peak at $T_N \approx 0.95$ K . Below T_N, a linear extrapolation of the C_p/T versus T^2 plot shown in the inset of Fig. 6(a) below 0.4 K^2 yields $\gamma \approx 0$ mJ mol^{-1} K^{-2}. This is considerably smaller than the earlier reported value of $\gamma \approx 300$ mJ mol^{-1} K^{-2} [28]. Likewise, the value of the Sommerfeld coefficient γ estimated from a linear fit of C_p/T versus T^2 in the paramagnetic state between $T^2 = 65$ and 500 K^2 [inset of Fig. 6(b)] yields an equally small value $\gamma = 6$ mJ mol^{-1} K^{-2}.

The magnetic contribution $C_m(T)$ to the specific heat of CePtPb can be approximated by taking the difference between the specific heat of CePtPb and LaPtPb. The obtained $C_m(T)$ [Fig. 6(b)] exhibits a sharp peak at T_N with a tail that extends up to $T \approx 20$ K and a broad local maximum around 100 K. The broad maximum is due to the CEF effect, whereas the large specific heat below $T \approx 10$ K is likely due to a Kondo contribution or short-range magnetic correlations.

Figures 7(a) and 7(b) show $C_m(T)$ for various magnetic fields applied in the *ab* plane. The sharp peak at T_N for zero field broadens and shifts to lower temperature as the magnetic field is increased [Fig. 7(a)]. At $H = 6$ kOe, no peak indicative of magnetic order is observed down to 0.4 K. For $H = 10$ kOe, a broad maximum in $C_m(T)$ is observed around $T = 1.2$ K, which further broadens and shifts to higher temperature as the magnetic field is increased to $H = 90$ kOe [Fig. 7(b)].

The magnetic field dependence of C_p/T for $T = 0.5$ K is shown in Figs. 7(c) and 7(d). Despite the scatter in the data points, it is clear that $C_p(H)/T$ increases gradually from 1.94 J mol^{-1} K^{-2} at $H = 0$ kOe to 2.3 J mol^{-1} K^{-2} at $H = 2.5$ kOe. Moreover, $C_p(H)/T$ decreases rapidly as the magnetic field is increased up to 90 kOe.

Figure 8 shows the magnetic entropy $S_m(T)$, estimated by integrating C_m/T with respect to T above 0.4 K. To interpret the total magnetic entropy, the missing entropy below 0.4 K must be considered. In zero field, $0.4R \ln 2$ of the magnetic

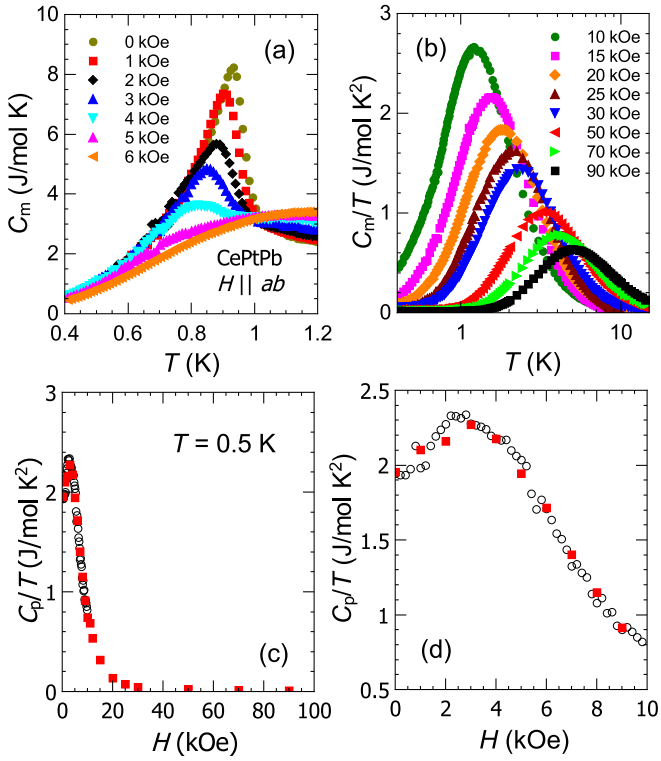

FIG. 7. (a) Temperature dependence of the magnetic contribution to the specific heat $C_m(T)$ of CePtPb for magnetic fields $H \leqslant 6$ kOe. (b) C_m/T vs T for $H \geqslant 10$ kOe. (c) Magnetic field dependence of the specific heat $C_p(H)$ of CePtPb at $T = 0.5$ K, plotted as C_p/T vs H (open circles). Data taken from $C_p(T)$ at $T = 0.5$ K for constant magnetic field (solid squares) are also shown. (d) The data from (c) for $H \leqslant 10$ kOe.

entropy is recovered at T_N. Above 5 K, the magnetic entropy first approaches saturation near $R\ln 2$ (Fig. 8 inset), suggesting CePtPb has a doublet ground state. As shown in the inset of Fig. 6(a), the missing entropy below 0.4 K can be estimated from an extrapolation of the data for $C_p(T)/T$ to $T = 0$ K assuming $C_p(T)/T \propto T^2$ below $T^2 = 0.4$ K^2. In this approximation, $R\ln(2)$ is recovered at $T \approx 10$ K . Above 25 K, $S_m(T)$ increases with temperature up to 300 K, passing through the value $R\ln 4$ at $T \approx 225$ K . The temperature dependence of $S_m(T)$ for different applied magnetic fields is shown in the inset of Fig. 8. For $H \geqslant 10$ kOe, the recovery to $R\ln(2)$ is pushed to higher temperatures, which is consistent with Zeeman splitting of the ground state doublet.

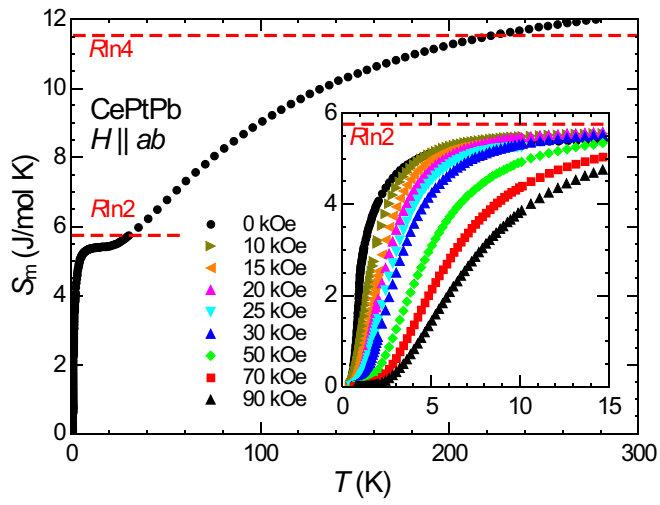

FIG. 8. Magnetic entropy $S_m(T)$ for CePtPb at $H = 0$ kOe. The inset shows $S_m(T)$ for different applied magnetic fields.

D. Muon spin relaxation

Representative zero-field (ZF) μSR asymmetry spectra $A(t)$ for CePtPb at various temperatures are shown in Fig. 9. The first 0.03 μs of the spectra are contaminated by positive muons (μ^+) that missed the sample and directly triggered the positron detectors, and consequently has been removed.

Above T_N, the asymmetry spectra are well described by the product of an exponential relaxation function and a temperature independent Gaussian Kubo-Toyabe function [30], the latter intended to account for a nuclear-dipolar contribution [31]. Specifically,

$$A(t) = A_S e^{-\lambda t} G_{GKT}(\Delta, t) + A_B \,, \qquad (1)$$

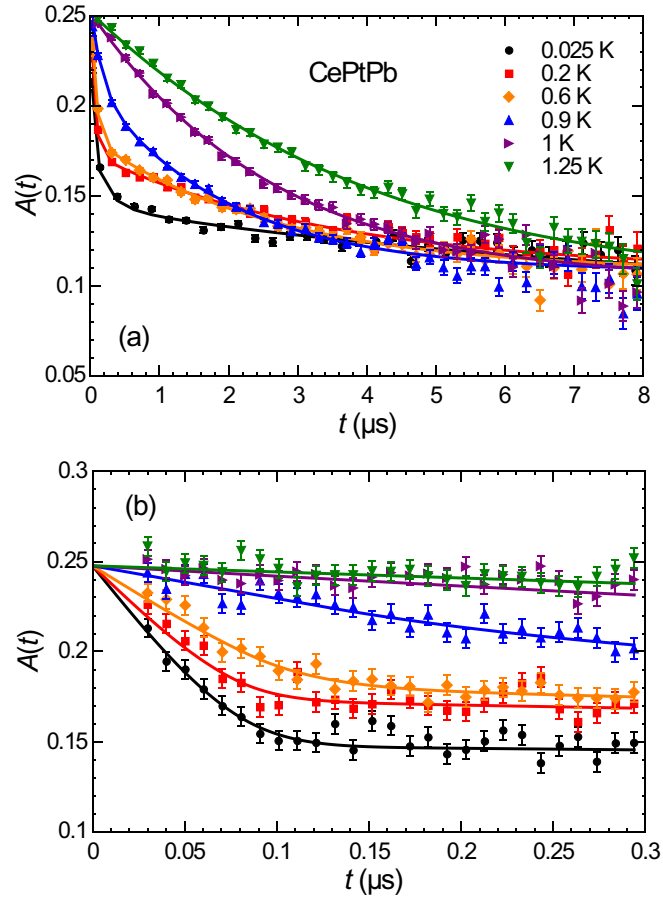

FIG. 9. ZF-μSR asymmetry spectra for CePtPb at various temperatures recorded with the initial muon spin polarization $\mathbf{P}(0)$ parallel to the ab plane, plotted over the first (a) 8 and (b) 0.3 μs. The solid curves are fits to Eqs. (1) and (2) as described in the main text.

where $G_{\rm GKT}(t) = \frac{1}{3} + \frac{2}{3}(1-\Delta^2 t^2)e^{-\frac{1}{2}\Delta^2 t^2}$ is a static Gaussian Kubo-Toyabe function. Δ^2/γ_μ^2 is the second moment of the internal static magnetic field distribution, assumed to be Gaussian. The muon gyromagnetic ratio is denoted by γ_μ. $A_{\rm S}$ and $A_{\rm B}$ are the sample and background contributions to the initial asymmetry, respectively. This is an example of double relaxation, where the muon is sensitive to the combined nuclear and electronic contributions, only because the system is in the rapidly fluctuating paramagnetic regime and λ is small. The background component arises primarily from muons that missed the CePtPb sample and stopped in the Ag sample holder. The relaxation function $G_{\rm GKT}(\Delta, t)$ is intended to account for the nuclear dipole moments in CePtPb, which are randomly oriented and static on the μSR time scale. Fits assuming $G_{\rm GKT}(\Delta, t)$ is independent of temperature yield $\Delta = 0.07\ \mu{\rm s}^{-1}$. The exponential function $\exp(-\lambda t)$ in Eq. (1) accounts for the relaxation of the ZF-μSR signal by the Ce-4f electronic moments.

Below $T_{\rm N}$, a rapid decrease of $A(t)$ occurs in the first 0.1 μs. To account for this, the asymmetry spectra below $T_{\rm N}$ were fit assuming the sample contribution is described by the sum of slow-relaxing and fast-relaxing exponential functions

$$A(t) = A_1 e^{-\lambda_1 t} + A_2 e^{-\lambda_2 t} + A_{\rm B}\,, \qquad (2)$$

where $A_1 + A_2 = A_{\rm S}$.

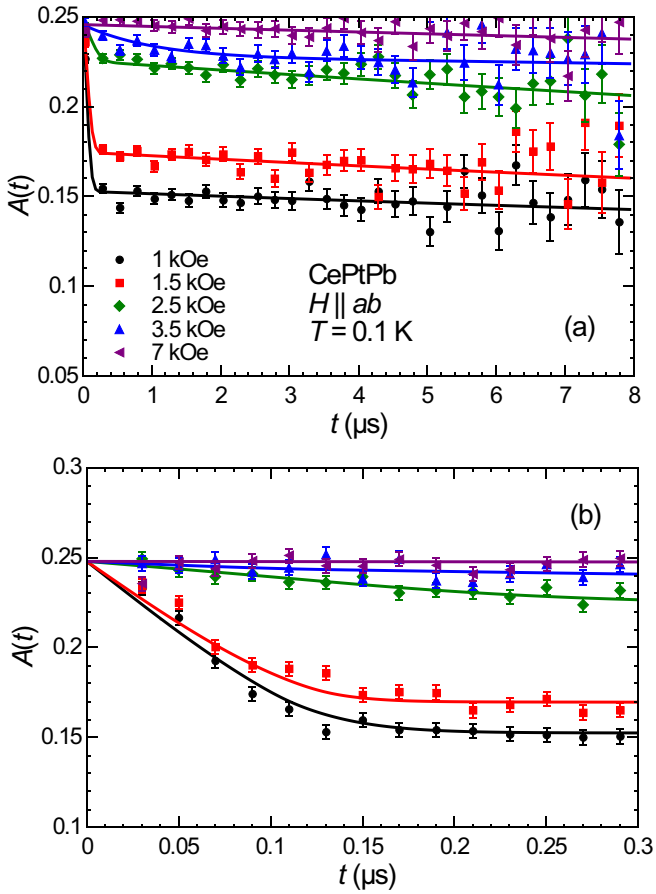

FIG. 10. LF-μSR asymmetry spectra for CePtPb at $T = 0.1$ K recorded with the initial muon spin polarization $\mathbf{P}(0)$ parallel to the *ab* plane, plotted up to (a) 8 and (b) 0.3 μs. The solid curves are fits to Eqs. (1) and (2) as described in the main text.

Figure 10 shows longitudinal-field (LF) μSR asymmetry spectra for CePtPb at $T = 0.1$ K for a field applied in the *ab* plane. The fast relaxing contribution to $A(t)$ is continuously suppressed by the increasingly large applied magnetic field. For $H \geqslant 3.5$ kOe, the sample contribution to $A(t)$ is well described by a single exponential relaxation function—that is, Eq. (1) with $G_{\rm GKT}(\Delta, t) = 1$. The temperature dependence of the fit parameters for the ZF-μSR and LF-μSR measurements are shown in Figs. 11 and 12, respectively.

Above $T_{\rm N}$, the ZF exponential relaxation rate λ increases as the temperature is lowered towards $T_{\rm N}$ [Fig. 11(b)] due to a slowing down of Ce-4f spin fluctuations. Below $T_{\rm N}$ where the sample contribution to the ZF-μSR asymmetry spectrum $A(t)$ develops two exponential components [Fig. 11(a)], the amplitude of the slower relaxing component A_1 and the corresponding relaxation rate λ_1 decrease with decreasing temperature. At $T = 0.025$ K, $\lambda_1 = 0.25\ \mu{\rm s}^{-1}$ and A_1 becomes 37% of the total sample asymmetry $A_{\rm S}$ [Fig. 11(b)]. Together the sharp rise in λ near $T_{\rm N}$ and subsequent decrease of λ_1 below $T_{\rm N}$

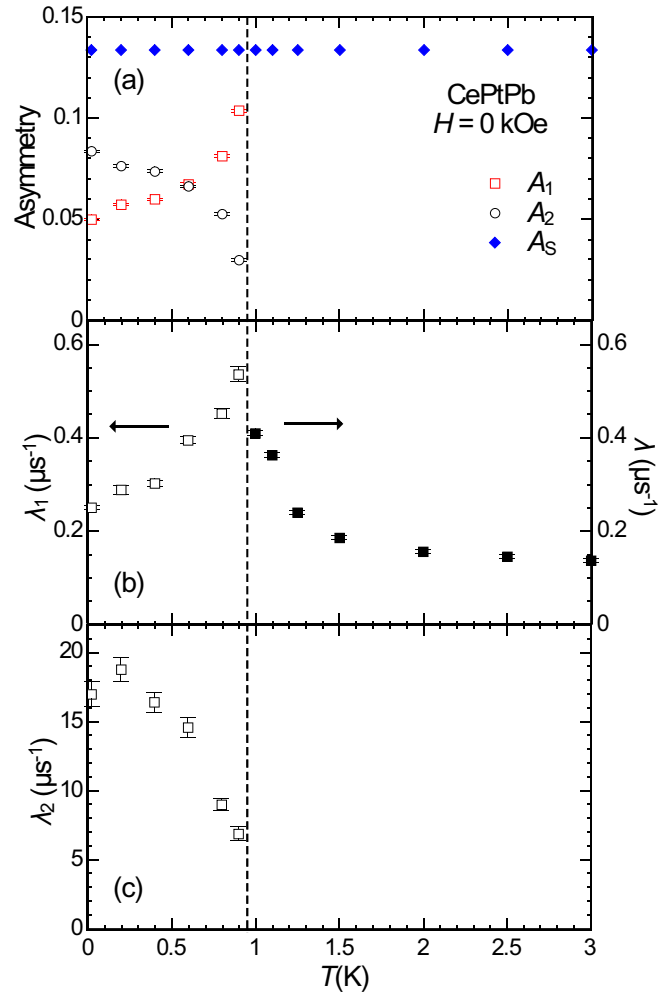

FIG. 11. Temperature dependence of the ZF-μSR fit parameters for CePtPb. (a) The total signal amplitude $A_{\rm S}$ and the amplitudes A_1 and A_2 of the slow-relaxing and fast-relaxing exponential components below $T_{\rm N}$. (b) The exponential relaxation rates λ (right axis) and λ_1 (left axis), and (c) λ_2. The dashed vertical line indicates $T_{\rm N}$ for zero field.

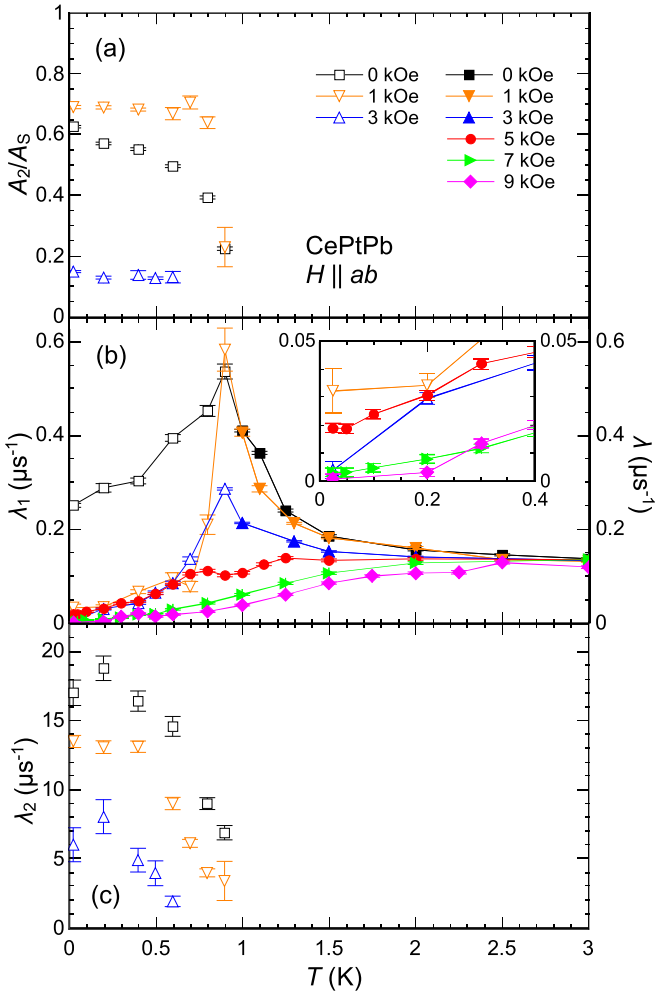

FIG. 12. Temperature dependence of the ZF- and LF-μSR fit parameters for CePtPb. (a) The normalized asymmetry A_2/A_S associated with the fast-relaxing exponential sample component. (b) The exponential relaxation rates λ (closed symbols) and λ_1 (open symbols). The inset shows a blow up of the plot below 0.4 K. (c) Exponential relaxation rate λ_2 associated with the fast-relaxing sample component.

form a peak that is indicative of a magnetic phase transition. The nonzero value of λ_1 for 0.025 K, however, suggests that slow Ce-4f spin fluctuations persist in part of the sample. In contrast to A_1, the amplitude of the fast-relaxing exponential component A_2 increases below T_N, reaching 63% of A_S at $T = 0.025$ K [Fig. 12(a)]. The corresponding relaxation rate λ_2 increases in value to 17 μs^{-1} [Fig. 11 (c)], which is indicative of a broad internal magnetic field distribution.

The ratio of A_2/A_S at $T = 0.025$ K increases slightly to 69 % upon application of a longitudinal field $H = 1$ kOe, but is drastically reduced to 15 % for $H = 3$ kOe [Fig. 12(a)]. The peak formed by λ and λ_1 is suppressed by the field [Fig. 12(b)]. The absence of a peak for $H \geqslant 7$ kOe is consistent with the absence of any signature of magnetic order in the resistivity and specific heat measurements. The relaxation rate λ_2 is also suppressed by the longitudinal field [Fig. 12(c)]. A fast-relaxing component is not discernible for $H > 3$ kOe, indicating that in this field range the external field dominates the vector sum of the applied longitudinal field and the local field transverse to the muon spin polarization.

IV. DISCUSSION

A temperature versus magnetic field (T-H) phase diagram for CePtPb subject to a field $H \parallel ab$ can be constructed from the anomalous features observed in the resistivity and specific heat measurements. The onset of AFM order is evident from the observed peak in the $C_m(T)$ data shown in Figs. 6 and 7. The onset of AFM order is also indicated by peaks and kinks in the temperature and field derivatives of the resisitivity $\rho(T, H)$, as shown in Fig. 13(a)–13(c). For $H \geqslant 6$ kOe, however, the observed broad maximum in $d\rho(T)/dT$ shifts to higher temperature as the magnetic field is increased [Fig. 13(d)].

Figure 14 shows the T-H phase diagram constructed from the features in the $C_m(T, H)$ and $\rho(T, H)$ data. The AFM transition temperature T_N in zero field is continuously suppressed by magnetic field to $T = 0.4$ K at $H_c \approx 6$ kOe, with multiple phase transitions or crossovers within the magnetically ordered phase. Such is also the case for the isostructural compounds CePdAl and YbAgGe. Below T_N hysteresis is observed in CePtPb in the two intermediate phases between 0.8 and 3.5 kOe, which is indicated by the shaded region in

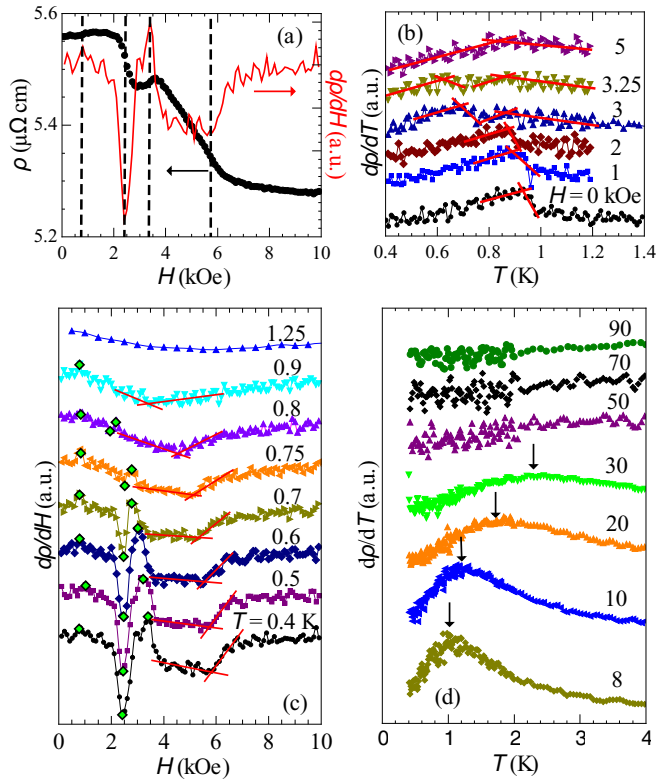

FIG. 13. (a) $\rho(H)$ (left axis) and $d\rho/dH$ (right axis) at $T = 0.4$ K . Vertical lines indicate a phase transition fields. (b) $d\rho/dT$ at selected magnetic fields. Solid lines are guides to the eye. (c) $d\rho/dH$ at selected temperatures. Solid lines are guides to the eye. (d) $d\rho/dT$ at various magnetic fields. Vertical arrows indicate a local maximum in $d\rho/dT$.

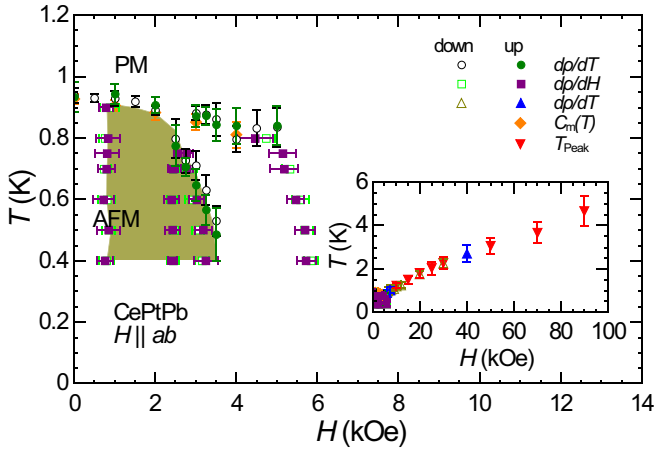

FIG. 14. T-H phase diagram of CePtPb for $H \parallel ab$, obtained from the $\rho(T, H)$ and $C_p(T, H)$ measurements. A shaded area represents a region where hysteresis is observed. The peak of a broad local maximum observed in $C_m(T)$ and $d\rho/dT$ for $H > H_c$ is plotted in the inset.

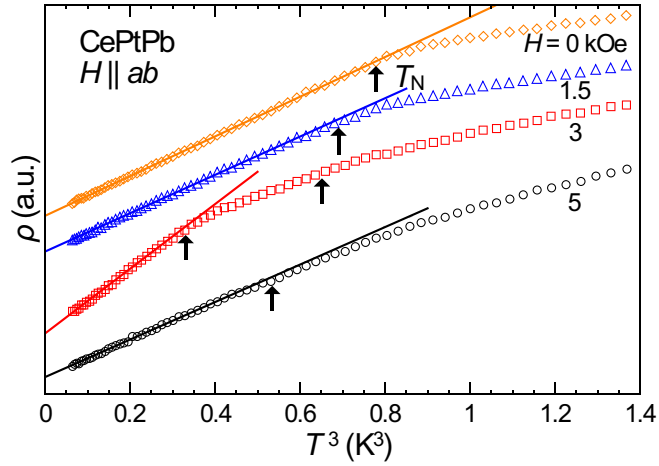

FIG. 15. Temperature dependence of the resistivity plotted vs T^3 at selected magnetic fields. Vertical arrows indicate the phase transition temperatures. Solid lines are linear fits to the data below T_N. For $H = 3$ kOe, $\rho(T)$ exhibits two magnetic transitions with decreasing temperature (Fig. 14). The fit was performed on the data only below the second transition.

Fig. 14. In contrast to YbAgGe [14,15], however, hysteresis is not observed for zero field. This is also the case for CePdAl, where hysteresis is observed in two intermediate phases well above zero field [22]. Based on an Ising-like, large magnetic anisotropy of the Ce-4f spins for low field, these phases in CePdAl are proposed to be canted AFM phases with spin-flop transitions occurring at the phase boundaries. Given that the magnetic susceptibility of CePtPb also exhibits a large anisotropy, it is likely that the hysteretic intermediate phases shown in Fig. 14 are also canted AFM phases.

The ZF-μSR measurements on CePtPb indicate there are residual spin dynamics at 0.025 K (Fig. 11). The temperature dependence of the sample component amplitudes A_1 and A_2 below T_N are compatible with two different scenarios. The first is that there is a gradual reorientation of the Ce-4f spins with decreasing temperature, which results in a variation of the orientation of the average local field with respect to the initial muon spin polarization $\mathbf{P}(0)$. In this case, λ_1 and λ_2 originate from components of the local field parallel and perpendicular to $\mathbf{P}(0)$, respectively. The second, and more likely scenario, is that inhomogeneous freezing occurs below T_N, where some fraction of the sample contains Ce-4f spins that do not freeze. In this picture, the two sample components in Eq. (2) are associated with spatially distinct magnetic contributions, with the slow (fast) relaxation rate λ_1 (λ_2) due to the fluctuating spins (spins that freeze). The temperature variation of the amplitudes A_1 and A_2 reflect the volume fraction of the sample containing fluctuating and frozen spins, respectively. The increase in A_2 and corresponding decrease in A_1 with decreasing temperature indicates a growth in the volume fraction of frozen Ce-4f spins. At 0.025 K, the amplitude ratios $A_2/A_S = 63\%$ and $A_1/A_S = 37\%$ suggest that two thirds of the Ce-4f spins order antiferromagnetically, while the other third remain fluctuating due to geometrical frustration. This interpretation assumes the magnetic structure is similar to that proposed for the related CePdAl compound [20,21,32]. The increase in A_2/A_S and significant drop in λ_1 between zero field and $H = 1$ kOe for $T < T_N$ (Fig. 12) suggests a partial alleviation of the magnetic frustration by the applied field as observed in CePdAl by neutron scattering [33].

The lower A_2/A_S ratio at $H = 3$ kOe [Fig. 12(a)] may be due to a Ce-4f spin reorientation, because a phase boundary is apparently crossed when the magnetic field is increased from 1 to 3 kOe (Fig. 14). In addition, the drop in A_2 likely has a contribution due to the fact that the external and internal static magnetic fields are now comparable, leading to decoupling [31]. The component of the internal magnetic field which is static may be estimated from $\lambda_2 \sim \gamma_\mu \Delta$, or roughly 1475 Oe. We note that μSR experiments performed with a weak magnetic field applied transverse to $\mathbf{P}(0)$ have the potential to confirm whether there is phase separation below T_N associated with frozen and unfrozen spins.

In zero field, a power-law analysis of the electrical resistivity $\rho(T) = \rho_0 + AT^n$ for CePtPb yields an exponent $n \approx 3$ below T_N, as shown in Fig. 4(d). Figure 15 shows that a similar value of n is observed for all of the magnetically ordered phases of CePtPb. This is also the case for the magnetically ordered phases of CePdAl [22].

For $H \gtrsim H_c$, the power-law analysis of the resistivity shows an anomalous evolution of the exponent n as a function of magnetic field. The fitting curves at selected magnetic fields are shown in Figs. 16(a)–16(c), and the field dependence of the fit parameters ρ_0, n, and A are shown in Figs. 16(d)–16(f). The data were fit over the temperature interval (0.4 K, T_{max}), where T_{max} increases with magnetic field as shown in the inset of Fig. 16(e). The field dependence of ρ_0 follows the $\rho(H)$ curve at $T = 0.4$ K for $H \gtrsim 20$ kOe [Fig. 16(d)], and the resistivity exponent n grows from $n \approx 2.5$ at H_c to $n \approx 4$ at $H = 90$ kOe [Fig. 16(e)]. A similar field-induced enhancement of n is observed in the Kondo lattice systems CePdAl [22], $CeAuSb_2$ [34], $CeNiGe_3$ [35], and $YbNi_4Cd$ [36]. In $CeAuSb_2$, a resistivity exponent $n \approx 1$ was observed below 3 K near a critical field $H_c = 55$ kOe [34].

Above H_c, n was observed to rapidly increase and saturate to $n = 3$ near $H = 70$ kOe. For $H > 70$ kOe, the temperature range where $n = 3$ behavior is observed appears to increase linearly with magnetic field, up to at least $H = 250$ kOe. It is suggested in Ref. [34] that the saturation to $n = 3$ is related to the alignment of the Ce-4f spins by the applied field, as both n and the magnetization appear to saturate at about the same field. By comparison, the value of n for $CeNiGe_3$ grows from $n = 2$ at H_c to $n \approx 3.8$ at $H = 90$ kOe with no sign of saturation [35], $n > 2$ is observed for CePdAl over the entire field range [22], and n for $YbNi_4Cd$ grows from $n = 2$ at H_c to the saturated value $n \approx 4$ at $H \gtrsim 30$ kOe [36]. For CePdAl, an exponent $n > 2$ for $H > H_c$ has been proposed to be due to spin dependent scattering of the quasiparticles in the saturated paramagnetic state [22].

Figure 16(f) shows that the field dependence of the resistivity coefficient $A = (\rho(T) - \rho_0)/T^n$ for CePtPb diverges near the critical field H_c. Such behavior is also observed in $CeAuSb_2$ [34], $CeNiGe_3$ [35], CePdAl [22], and $YbNi_4Cd$ [36]. In several magnetic field tuned QCP systems, a diverging field-dependent coefficient $A = (\rho(T) - \rho_0)/T^2$ is observed approaching H_c [37–39]. For CePtPb and CePdAl [22], neither Fermi liquid ($n = 2$) nor NFL ($n < 2$) behavior is observed close to H_c. This is also different than YbAgGe, where NFL behavior is observed near $H_c = 45$ kOe that extends over a wide range of field up to $H = 105$ kOe before Fermi liquid behavior is recovered [15].

To estimate the CEF energy level splitting, we have fit the broad maximum in the temperature dependence of C_m assuming the Schottky anomaly is described by a three doublet energy-level scheme. The fit curve $C_{Sch}(T)$ shown as a dashed curve in Fig. 17(a), corresponds to energy level splittings $\Delta_1 \approx 170$ K and $\Delta_2 \approx 330$ K . This result is qualitatively consistent with the development of anisotropy in the bulk magnetic susceptibility below 150 K (Fig. 3). Although such

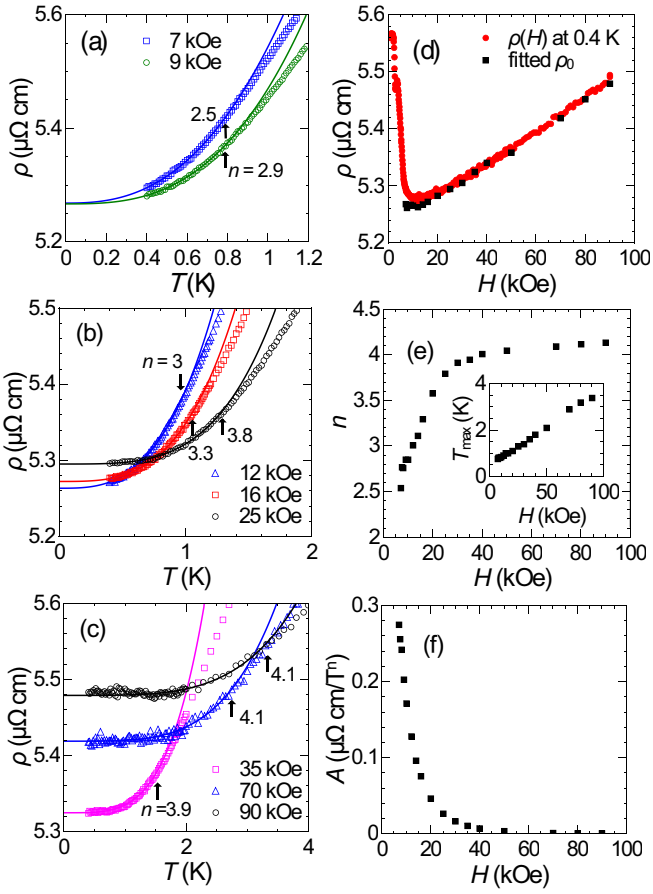

FIG. 16. Temperature dependence of the resistivity for applied magnetic fields of (a) 7 and 9 kOe, (b) 12, 16, and 25 kOe, and (c) 35, 70, and 90 kOe. The solid curves in (a)–(c) are fits to $\rho(T) = \rho_0 + AT^n$ over the temperature interval (0.4 K, T_{max}), where the temperature T_{max} is indicated by the vertical arrows and the values of n are shown in each panel. The dependence of the fitting parameters ρ_0, n, and A on the applied magnetic field are shown in (d)–(f), respectively. In addition, the field dependence of the resistivity at $T = 0.4$ K is also shown in (d), and the inset of (e) shows the magnetic field dependence of T_{max}.

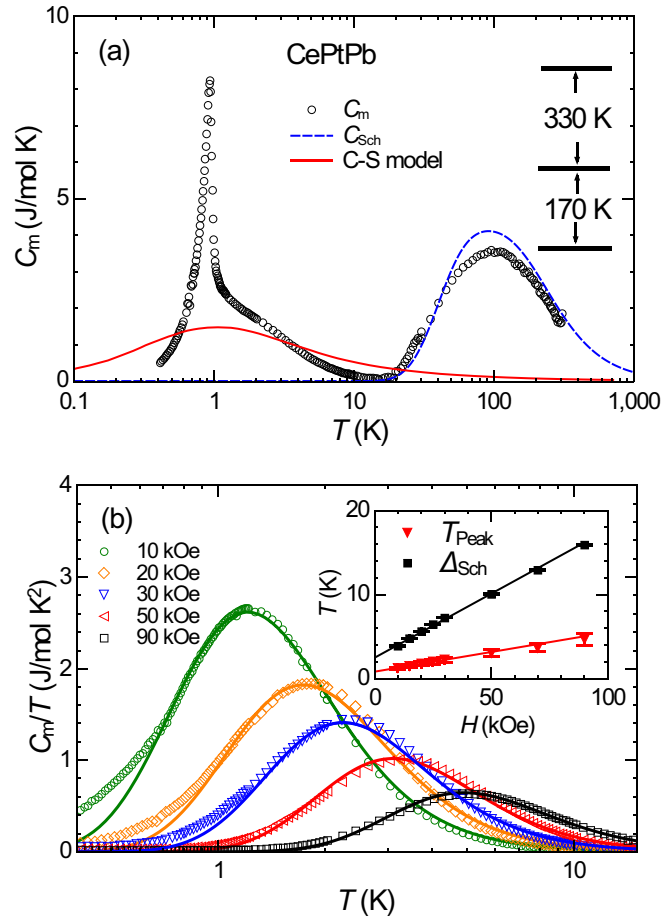

FIG. 17. (a) Magnetic contribution to the zero-field specific heat of CePtPb. The red curve represents the $J = 1/2$ Coqblin-Schrieffer model [41] with the scaling temperature $T_0 = 1.2$ K . The dashed curve is a fit to a three-level Schottky contribution with $\Delta_1 = 170$ K and $\Delta_2 = 330$ K . (b) C_m/T data for $H \gtrsim 10$ kOe. The solid curves represent an electronic Schottky contribution associated with Zeeman splitting of the ground-state CEF doublet by Δ_{Sch}. Inset shows the magnetic field dependences of Δ_{Sch} and the temperature of the broad maximum T_{Peak}. The solid lines in the inset are guides to the eye.

analysis achieves only qualitative agreement, it is sufficient to establish that the ground-state CEF doublet is well separated from the first-excited state.

For a Kondo lattice system, the Kondo temperature can be estimated from the magnetic entropy, where $S_m(T_K) \approx 0.7R\ln(2)$ [40]. This yields $T_K \approx 2$ K, which is consistent with the previous study of CePtPb [28]. However, the approximate value of the electronic specific heat coefficient γ determined from our measurements of C_p/T versus T^2 is much smaller than the value estimated from T_K, indicating that the $4f$ electrons in CePtPb are weakly hybridized with the conduction electrons. To investigate whether the heavy fermion behavior coexists with antiferromagnetism in CePtPb, the magnetic part of the specific heat for CePtPb was compared to the Coqblin-Schrieffer model [41] for a $J = 1/2$ doublet ground state. As shown in Fig. 17(a), the magnitude and width of the specific heat below 10 K is not described by this model. Alternatively, strong magnetic fluctuation can also produce such a large C_m in frustrated system such as CePdAl [23]. The frustration parameter $\theta_p/T_N \approx 40$ for CePtPb is sufficiently large to infer that magnetic frustration is dominant at low temperatures. In this case the gradual recovery of the full $R\ln(2)$ magnetic entropy by 10 K may be ascribed to geometric frustration of the Ce-$4f$ moments in the quasikagome lattice, which is supported by the μSR analysis.

Figure 17(b) shows the temperature dependence of C_m/T in the paramagnetic state for $H \geqslant 10$ kOe. The broad peak observed at low temperatures shifts to higher temperature with increased magnetic field. Consequently, we attribute the peak to an electronic Schottky contribution associated with Zeeman splitting of the ground state CEF doublet. Consistent with this interpretation, both the temperature of the local maximum (denoted by T_{Peak}) and the energy level splitting of the ground-state doublet (Δ_{Sch}) increase linearly with magnetic field [Fig. 17(b) inset]. The C_m/T data above the maximum are well described by the electronic Schottky contribution, whereas below the maximum there is clearly an additional contribution of some kind. The difference between the magnetic and Schottky contributions to the specific heat $(C_m - C_{Sch})/T$ may be regarded as an electronic contribution. Figure 18 shows the dependence of $(C_m - C_{Sch})/T$ on temperature and magnetic field. Although a clear signature of NFL behavior (i.e., $\propto -\log T$) is not observed near the critical field H_c (Fig. 18 inset), measurements at lower temperature may reveal something different. At $H = H_c(T = 0.4\,\text{K})$, $(C_m - C_{Sch})/T$ has a large value of $0.56\,\text{J mol}^{-1}\,\text{K}^{-2}$ that rapidly decreases with increasing magnetic field. This behavior suggests a field-induced suppression of the Kondo effect, as observed in other heavy-fermion systems [37,39]. On the other hand, such behavior could be due to a suppression of the magnetic fluctuations by the applied field. Further experimental studies below 0.4 K are needed to clarify the interplay between the effect of Kondo screening and geometrical frustration on the magnetic properties of CePtPb.

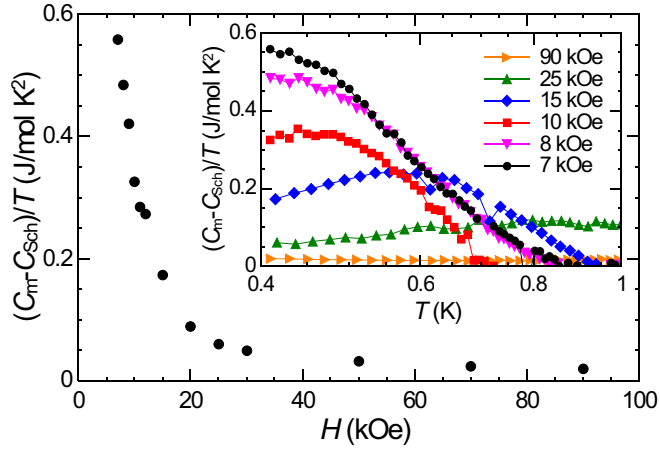

FIG. 18. Magnetic field dependence of $(C_m - C_{Sch})/T$ for $T = 0.4$ K . Inset shows the temperature dependence of $(C_m - C_{Sch})/T$ for selected applied magnetic fields.

V. SUMMARY

We have grown single crystals of CePtPb, which crystallize in the hexagonal ZrNiAl-type structure with the Ce ions presumably forming a quasikagome lattice in the *ab* plane. A T-H phase diagram has been constructed from measurements of the electrical resistivity and specific heat, which at low temperatures are strongly dependent on the external magnetic field. The zero-field AFM transition $T_N = 0.95$ K is suppressed by the applied field and vanishes at a critical field $H_c \approx 6$ kOe. Within the AFM phase, there are successive field-induced modifications of the magnetic order. Near H_c, neither the resistivity nor the magnetic contribution to the specific heat exhibit standard NFL behavior [i.e., $\rho(T) \propto T$ or $C_m(T) \propto -\log(T)$]. The resistivity exhibits a power-law dependence on temperature with an exponent $n > 2$ in both the magnetically ordered and paramagnetic states. Our ZF-μSR measurements indicate residual spin dynamics for $T = 0.025$ K, and by analogy with CePdAl are consistent with only two thirds of the Ce-$4f$ spins participating in the AFM order while the other third fluctuate. Lastly, our results suggest that the low-temperature physical properties of CePtPb are influenced by geometrical frustration.

ACKNOWLEDGMENTS

This work was supported by the Canada Research Chairs program, the Natural Science and Engineering Research Council of Canada, the Canadian Institute for Advanced Research, and the Canadian Foundation for Innovation.

[1] G. R. Stewart, Rev. Mod. Phys. **56**, 755 (1984).
[2] A. C. Hewson, *The Kondo Problem to Heavy Fermions* (Cambridge University Press, Cambridge, 1997).
[3] S. Doniach, Physica B&C (Amsterdam) **91**, 231 (1977).
[4] G. R. Stewart, Rev. Mod. Phys. **73**, 797 (2001).
[5] G. R. Stewart, Rev. Mod. Phys. **78**, 743 (2006).
[6] P. Gegenwart, Q. Si, and F. Steglich, Nat. Phys. **4**, 186 (2008).

[7] Q. Si, S. Rabello, K. Ingersent, and J. L. Smith, Nature (london) **413**, 804 (2001).

[8] Q. Si, Phys. B Condens. Matter **378-380**, 23 (2006).

[9] Q. Si, Phys. Status Solidi B **247**, 476 (2010).

[10] P. Coleman and A. H. Nevidomskyy, J. Low Temp. Phys. **161**, 182 (2010).

[11] Y. Motome, K. Nakamikawa, Y. Yamaji, and M. Udagawa, Phys. Rev. Lett. **105**, 036403 (2010).

[12] B. H. Bernhard, B. Coqblin, and C. Lacroix, Phys. Rev. B **83**, 214427 (2011).

[13] Q. Si and S. Paschen, Phys. Status Solidi B **250**, 425 (2013).

[14] K. Umeo, K. Yamane, Y. Muro, K. Katoh, Y. Niide, A. Ochiai, T. Morie, T. Sakakibara, and T. Takabatake, J. Phys. Soc. Jpn. **73**, 537 (2004).

[15] S. L. Bud'ko, E. Morosan, and P. C. Canfield, Phys. Rev. B **69**, 014415 (2004).

[16] G. M. Schmiedeshoff, E. D. Mun, A. W. Lounsbury, S. J. Tracy, E. C. Palm, S. T. Hannahs, J.-H. Park, T. P. Murphy, S. L. Bud'ko, and P. C. Canfield, Phys. Rev. B **83**, 180408(R) (2011).

[17] E. Mun, S. L. Bud'ko, and P. C. Canfield, Phys. Rev. B **82**, 174403 (2010).

[18] Y. Tokiwa, M. Garst, P. Gegenwart, S. L. Bud'ko, and P. C. Canfield, Phys. Rev. Lett. **111**, 116401 (2013).

[19] H. Kitazawa, A. Matsushita, T. Matsumoto, and T. Suzuki, Phys. B **199-200**, 28 (1994).

[20] A. Dönni, G. Ehlers, H. Maletta, P. Fischer, H. Kitazawa, and M. Zolliker, J. Phys.: Condens. Matter **8**, 11213 (1996).

[21] A. Oyamada, S. Maegawa, M. Nishiyama, H. Kitazawa, and Y. Isikawa, Phys. Rev. B **77**, 064432 (2008).

[22] H. Zhao, J. Zhang, S. Hu, Y. Isikawa, J. Luo, F. Steglich, and P. Sun, Phys. Rev. B **94**, 235131 (2016).

[23] S. Lucas, K. Grube, C.-L. Huang, A. Sakai, S. Wunderlich, E. L. Green, J. Wosnitza, V. Fritsch, P. Gegenwart, O. Stockert, and H. V. Löhneysen, Phys. Rev. Lett. **118**, 107204 (2017).

[24] V. Fritsch, N. Bagrets, G. Goll, W. Kittler, M. J. Wolf, K. Grube, C.-L. Huang, and H. V. Löhneysen, Phys. Rev. B **89**, 054416 (2014).

[25] M. S. Kim, Y. Echizen, K. Umeo, S. Kobayashi, M. Sera, P. S. Salamkha, O. L. Sologub, and T. Takabatake, X. Chen, T. Tayama, T. Sakakibara, M. H. Jung, and M. B. Maple, Phys. Rev. B **68**, 054416 (2003).

[26] A. Schenck, F. N. Gygax, M. S. Kim, and T. Takabatake, J. Phys. Soc. Jpn. **73**, 3099 (2004).

[27] Y. Tokiwa, C. Stingl, M. S. Kim, T. Takabatake, and P. Gegenwart, Sci. Adv. **1**, e1500001 (2015).

[28] R. Movshovich, J. M. Lawrence, M. F. Hundley, J. Neumeier, J. D. Thompson, A. Lacerda, and Z. Fisk, Phys. Rev. B **53**, 5465 (1996).

[29] P. C. Canfield and Z. Fisk, Philos. Mag. B **65**, 1117 (1992).

[30] T. Yamazaki, Hyperfine Interact. **65**, 757 (1991).

[31] R. S. Hayano, Y. J. Uemura, J. Imazato, N. Nishida, T. Yamazaki, and R. Kubo, Phys. Rev. B **20**, 850 (1979).

[32] V. Fritsch, S. Lucas, Z. Huesges, A. Sakai, W. Kittler, C. Taubenheim, S. Woitschach, B. Pedersen, K. Grube, B. Schmidt, P. Gegenwart, O. Stockert, and H. V. Löhneysen, J. Phys.: Conf. Ser. **807**, 032003 (2017).

[33] K. Prokeš, P. Manuel, D. T. Adroja, H. Kitazawa, T. Goto, and Y. Isikawa, Physica B: Condens. Matter **385-386**, 359 (2006).

[34] L. Balicas, S. Nakatsuji, H. Lee, P. Schlottmann, T. P. Murphy, and Z. Fisk, Phys. Rev. B **72**, 064422 (2005).

[35] E. D. Mun, S. L. Bud'ko, A. Kreyssig, and P. C. Canfield, Phys. Rev. B **82**, 054424 (2010).

[36] J. Lee, H. Park, N. R. Lee-Hone, D. M. Broun, and E. Mun, Phys. Rev. B **97**, 195144 (2018).

[37] P. Gegenwart, J. Custers, C. Geibel, K. Neumaier, T. Tayama, K. Tenya, O. Trovarelli, and F. Steglich, Phys. Rev. Lett. **89**, 056402 (2002).

[38] J. Paglione, M. A. Tanatar, D. G. Hawthorn, E. Boaknin, R. W. Hill, F. Ronning, M. Sutherland, L. Taillefer, C. Petrovic, and P. C. Canfield, Phys. Rev. Lett. **91**, 246405 (2003).

[39] E. D. Mun, S. L. Bud'ko, C. Martin, H. Kim, M. A. Tanatar, J.-H. Park, T. Murphy, G. M. Schmiedeshoff, N. Dilley, R. Prozorov, and P. C. Canfield, Phys. Rev. B **87**, 075120 (2013).

[40] H.-U. Desgranges and K. D. Schotte, Phys. Lett. A **91**, 240 (1982).

[41] V. T. Rajan, Phys. Rev. Lett. **51**, 308 (1983).